NANO LETTERS
2005
Vol. 5, No. 1
157−161

Biological Behavior of Hat-Stacked Carbon Nanofibers in the Subcutaneous Tissue in Rats

Atsuro Yokoyama,*,† Yoshinori Sato,‡ Yoshinobu Nodasaka,† Satoru Yamamoto,† Takao Kawasaki,† Masanobu Shindoh,† Takao Kohgo,† Tsukasa Akasaka,† Motohiro Uo,† Fumio Watari,† and Kazuyuki Tohji‡

Graduate School of Dental Medicine, Hokkaido University, and Graduate School of Environmental Studies, Tohoku University

Received September 17, 2004; Revised Manuscript Received November 6, 2004

ABSTRACT

The tissue response to hat-stacked carbon nanofibers (H-CNFs) was evaluated. H-CNFs were implanted in the subcutaneous tissue of rats. Histological and ultrastructural investigations were carried out by transmission electron microscopy. Although many macrophages and foreign body giant cells were seen around H-CNFs, no severe inflammatory response such as necrosis was observed. Some H-CNFs were observed in lysosomal vacuoles of phagocytes. These results showed that H-CNFs were not strong prophlogistic substances and were englobed in vivo.

Medical applications of nanoscale substances such as carbon nanotubes (CNTs) and fullerenes have attracted a great deal of attention. In particular, nanoscale substances are indispensable for the development of new drug delivery systems and scaffolds. There have been some reports on the use of CNTs and fullerenes for biomaterials.[1−8] Most of them were studies in vitro such as on scaffolds for cell culture.[1−3, 5,6] Recently, toxicity of CNTs was reported, and their safety as biomaterials has been questioned.[9−20] Thus, the investigation of tissue responses, including in animal experiments in addition to in vitro studies, is necessary to evaluate toxicity and biocompatibility of nanoscale substances and to develop them for medical devices. However, there are only a few reports about tissue reactions to nanoscale substances.[11,12,19,20] We have studied nanocarbon materials as one of the nanoscale substances for biomaterials.[7,8,21,22] Sato et al. developed a colloidal dispersion of a new type of carbon nanofibers (CNFs) for application to biomaterials.[23] As their structure was similar to stacked hats, they named them hat-stacked carbon nanofibers (H-CNFs). H-CNFs with a novel graphene structure would be more suitable for biomaterials, because it is possible to control their size and to make them soluble in water. The purpose of this study was to investigate the tissue response in subcutaneous tissue and evaluate biocompatibility of H-CNFs for the first time.

H-CNFs were produced with a thermal CVD method using a powdered Ni catalyst in a conventional flow reactor system according to the report by Rodriguez.[24,25] The powdered Ni catalyst is placed in an Al_2O_3 boat positioned in a horizontal quartz tube furnace. The sample is initially reduced in a 10% hydrogen/helium stream for 120 min at 873 K. C_2H_4/H_2 (4:1) mixture gas is then introduced and reacted at 873 K for 4 h. Then, 100 mg of the produced soot is introduced into a flask with a reflux attachment together with 500 mL of 6 M hydrochloric acid for 12 h at 373 K. After HCl-reflux treatment, the suspension is filtered using a membrane filter with 0.1 μm apertures. Next, the filtered cake is transferred into a flask with 1.0 L of 6 M HNO_3 and refluxed at 373 K for 12 h to perfectly dissolve residual nickel. After the suspension is filtrated using a membrane filter of 0.1 μm apertures, the filtered cake is subsequently washed and finally dried for 24 h at 333 K. The measurement was carried out by scanning electron microscopy (SEM; S-4100, Hitachi, Japan) and transmission electron microscopy (TEM; HF-2000, Hitachi, Japan) in situ using energy-dispersive X-ray spectroscopy with ultrathin window, which is detectable for the atoms heavier than the atomic number 5 (B) (EDXS; Vantage EDX system, NORAN Instruments). The scheme, EDX analysis, SEM, and TEM of H-CNFs are shown in Figure 1. The structure of H-CNFs resembles bamboo hats stacked up toward a needle axis. Lengths of CNFs range approximately between 100 nm and 1 μm, and their diameters are between 30 and 100 nm, respectively. Ni was not detected by inductively coupled plasma optical emission spectrometry (ICP OES; Thermo elemental Co. Ltd., USA) and X-ray fluorescence analysis (XRF; MESA-500W, Horiba, Japan).

Eight male 6-week-old Wistar strain rats were used in this study. Under general anesthesia, incisions were made bilater-

* Corresponding author. Graduate School of Dental Medicine, Hokkaido University, Kita13, Nishi7,Kita-ku,Sapporo 060-8586, Japan. Tel: +81-11-706−4270. Fax: +81-11-706-4903. E-mail: yokoyama@den.hokudai.ac.jp
† Hokkaido University.
‡ Tohoku University.

10.1021/nl0484752 CCC: $30.25
Published on Web 12/08/2004

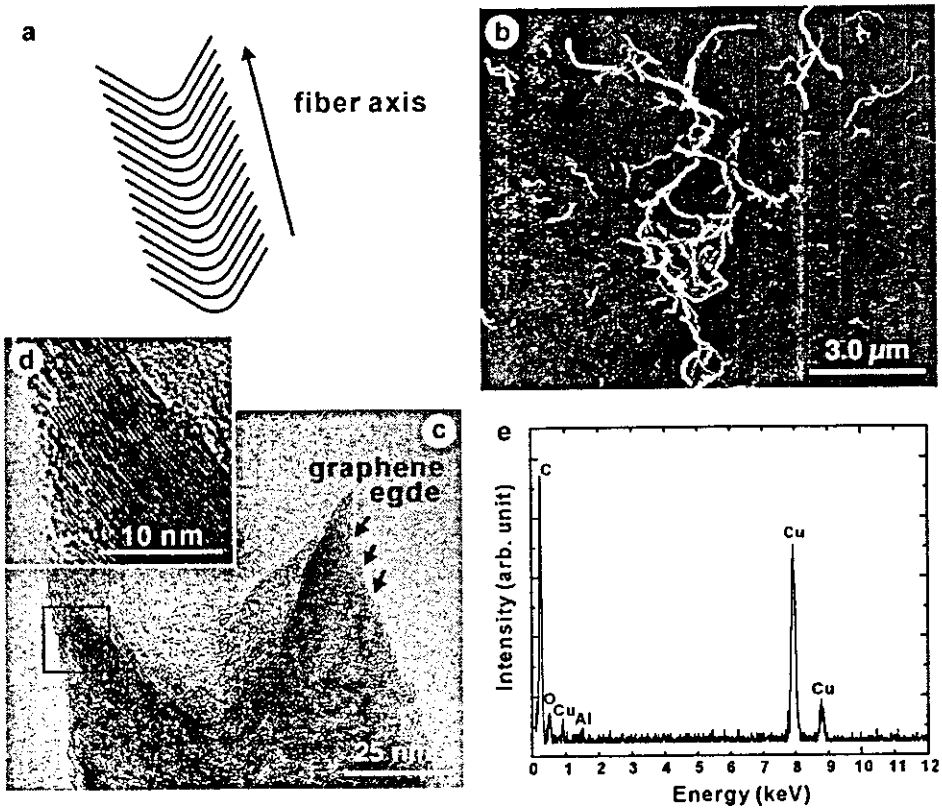

Figure 1. H-CNFs. (a) Scheme of H-CNFs. (b) SEM image of H-CNFs. (c) TEM image of CNFs. (d) High magnification of c. (e) EDX analysis of H-CNFs. The peaks of Cu and Al were due to the TEM grid made of cupper and the holder for the TEM grid, respectively.

ally in the thoracic region. Two pockets were made in the subcutaneous tissue. Clusters of H-CNFs were implanted in the subcutaneous tissue in the thoracic region bilaterally in each rat. Animal experiments were performed in accordance with the *Guide for the Care and Use of Laboratory Animals*, Hokkaido University Graduate School of Dental Medicine. During the course of the study, no rats were lost.

The rats were sacrificed at 1 and 4 weeks after surgery. Segments of the subcutaneous tissue including H-CNFs were excised and fixed. The fixed specimens were divided into two parts. One part was embedded in paraffin. Hematoxylin and eosin-stained specimens were observed by optical microscopy. The other was observed by TEM. The field observation by TEM was confirmed to be exactly consistent with that observed by optical microscopy. TEM specimens were postfixed with 1% OsO_4 and routinely embedded in epoxy resin after dehydration. Ultrathin sections (80 nm approximately) were cut with a diamond knife and stained with uranyl acetate and lead citrate. Stained sections were placed on a supporting carbon mesh grid and observed using a TEM operating at a voltage of 75 kV (H-800, Hitachi, Japan).

At 1 week after implantation, clusters of H-CNFs were surrounded by granulation tissue with a slight inflammatory change. Many mesenchymal cells, macrophages, and foreign body giant cells were observed around H-CNFs. The appearance was like foreign body granuloma (Figure 2a). High-magnification observation revealed that some H-CNFs were englobed by macrophages (Figure 2b). At 4 weeks, clusters of H-CNFs were surrounded by fibrous connective tissue (Figure 2c). Many foreign body giant cells were attached to H-CNFs (Figure 2d). No severe inflammatory response such as necrosis, degeneration, or neutrophil infiltration was observed around H-CNFs throughout the experimental period.

H-CNFs were observed in intercellular and intracellular spaces at 1 week after implantation (Figure 3a). Some of them were recognized in phagocytes with many vacuoles such as macrophages (Figure 3b). Lengths of H-CNFs were approximately between 100 nm and 1μm (Figure 3b). Many H-CNFs in phagocytes were aggregated (Figure 3c and d). Some H-CNFs in phagocytes were covered by a membrane (white arrows in Figure 3d), presumably a lysosomal membrane. There were no changes in the form of the H-CNFs after phagocytosis. The characteristic structures such as the stacked hats were still observed (Figure 3d).

At 4 weeks after implantation, H-CNFs were observed in phagocytes with a lot of vacuoles (Figure 4a). Although the characteristic form of H-CNFs, the hat-stacked shape, was recognized, the covering lysosomal membranes were seldom observed and the degree of aggregation was decreased (Figure 4b and c) in comparison with that at 1 week. Furthermore, H-CNFs looked shorter (Figure 4b) than those at 1 week and some H-CNFs appeared translucent (white arrow in Figure 4d), which was not observed at 1 week (Figure 4c and d).

Although it is desirable for carriers such as DDS and genes transfection to be water soluble, it is difficult to make CNTs soluble in water due to their chemical properties and shape with the μm length. H-CNFs have the characteristic structure that the edges of the stacked graphene layers are exposed at the surface. Therefore, many hydrophilic groups can be added

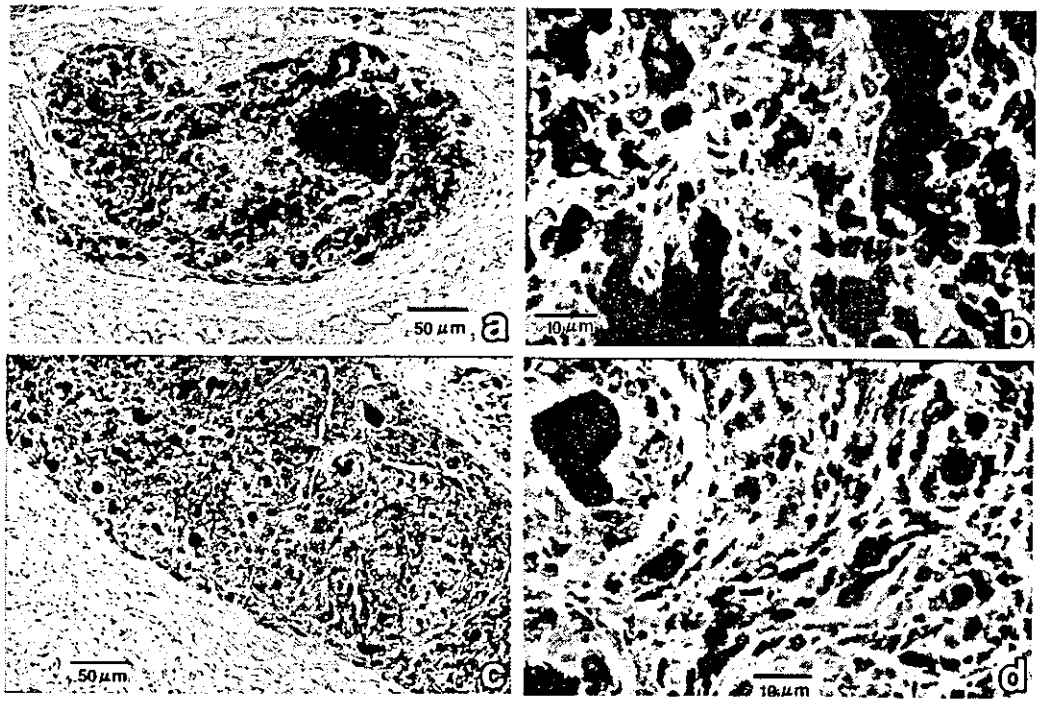

Figure 2. Histology of CNFs implanted in the subcutaneous tissue. (a) At 1 week. Clusters of CNFs were covered by granulation tissue. H. E. stain. (b) High magnification of a. Numerous macrophages and mesenchymal cells were observed around CNFs. (c) At 4 weeks. Clusters of CNFs were surrounded by fibrous connective tissue. H. E. stain. (d) High magnification of c. There were many foreign body giant cells attached to CNFs. H. E. stain.

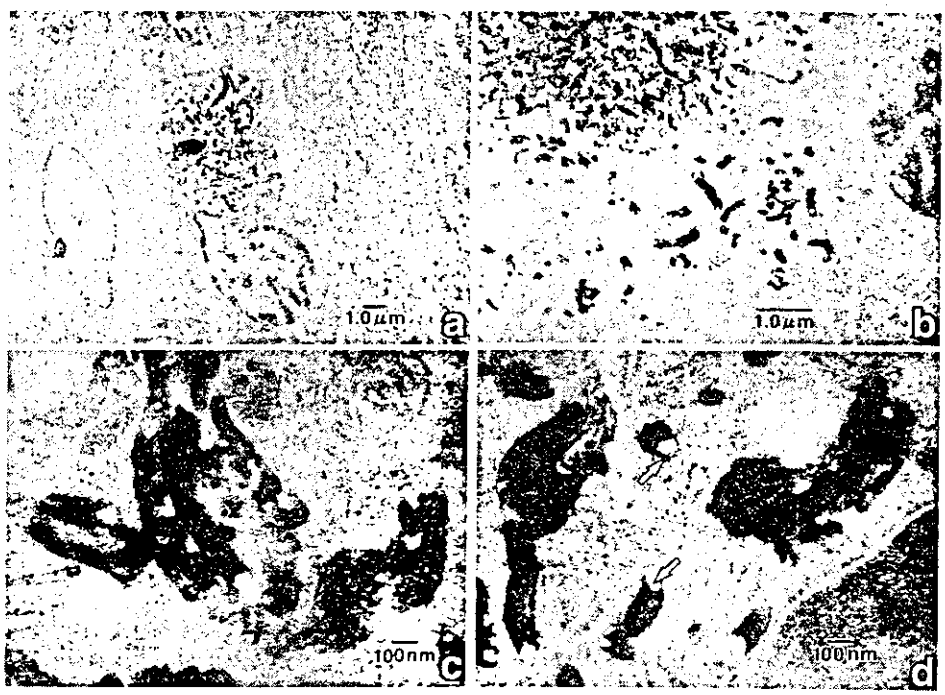

Figure 3. TEM images of CNFs implanted in the subcutaneous tissue at 1 week. (a) CNFs were observed in the cytoplasm of macrophage. (b) Various sizes of CNFs were observed in macrophage. (c) Many of CNFs in the phagocytes were aggregated. (d) Structure of membrane (white arrows) was observed around some of the CNFs.

and give water solubility to H-CNFs. Since the binding force between each graphene sheet originating from van der Waals force is rather weak, it is easy to cut and control the sizes of H-CNFs. Therefore, H-CNFs are suitable as a carrier of DDS and we investigated the tissue reaction of H-CNFs in this study.

The toxicity of nanoscale substances has been suggested recently.[9-20] Huczko et al. reported that CNTs containing soot synthesized from a catalyst-doped (Co/Ni) graphite anode by an arc discharge method did not induce any abnormalities of pulmonary function or measurable inflammation in guinea pigs, and that fullerene soot with a high

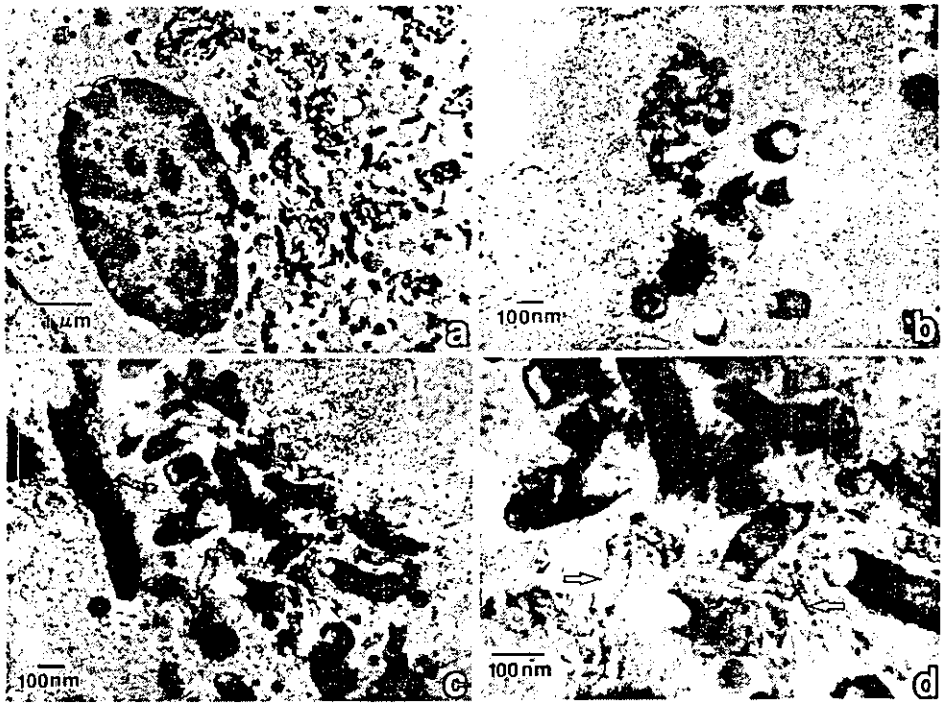

Figure 4. TEM images of CNFs implanted in the subcutaneous tissue at 4 weeks. (a) CNFs were observed in macrophage. (b) Smaller CNFs were observed compared with those at 1 week. (c) The degree of aggregation of CNFs was lower than that at 1 week. (d) Some CNFs (white arrows) became translucent.

content of single-walled carbon nanotubes (SWCNTs) did not induce any skin hazards.[11,12] On the other hand, Lam et al. investigated the pulmonary toxicity of SWCNTs using mice.[20] They reported that SWCNTs induced dose-dependent epithelioid granulomas and interstitial inflammation at 7 days, and peribronchial inflammation and necrosis at 90 days after intratracheal instillation, while carbon black as a control did not induce any severe inflammatory change. They considered that the difference of pulmonary toxicity between carbon nanotubes and carbon black was related to the physicochemical properties and fibrous structure of carbon nanotubes. Warheit et al. reported that SWCNTs instilled intratracheally induced granulomatous inflammation that was not dose dependent in rats, and that the cytotoxicity was perplexing.[21] In this study, although granulomatous inflammatory change around H-CNFs was observed at 1 week after implantation, they were surrounded by thin fibrous connective tissue at 4 weeks. These observations indicate that the organization process of inflammation for foreign bodies proceeded with time. Furthermore, no severe inflammatory response such as necrosis or invasion of neutrophils was observed. These results suggest that H-CNFs are not acutely toxic in the subcutaneous tissue. It seemed that wound healing was not inhibited, because slight inflammatory changes were observed only close to H-CNFs, while the control skin incisions were not done. These different results of our study from those of Lam et al. may be caused by the physicochemical properties of H-CNFs, for example, water solubility and the characteristic structure composed of the stacked graphene hats, apart from the implant site and species of the animals.

Observation by TEM revealed that H-CNFs implanted in the subcutaneous tissue were phagocytosed by macrophages. Foreign objects are englobed in macrophages in the inflammatory response. Titanium particles from dental and medical implants were recognized in macrophages by TEM observation in some reports.[26,27] Although cytostructures such as membranes of lysosomes were observed around most H-CNFs inside the phagocytes at 1 week, they were not observed at 4 weeks after implantation. The degree of aggregation of H-CNFs decreased from 1 week to 4 weeks. The H-CNFs appeared to become shorter with time, although quantification was not carried out. Furthermore, some of H-CNFs were translucent. These changes of structure in H-CNFs that occurred in lysosomes and cytoplasm might be related to the characteristics of H-CNFs. Delamination of layered materials by intercalation reactions has been reported.[28,29] In this study, delamination of graphene layers of H-CNFs could have originated from the intercalation of hydrophilic substances such as enzymes and proteins in lysosomes and cytoplasm related to rich functional groups resulting from exposure of the edges of the graphene hats. Decrease of fiber length of H-CNFs would occur subsequently. In addition, the energy of cytoplasmic motion[30] might be involved in the shortening of the H-CNFs in addition to the weak binding force between graphene sheet layers. The change of some of the H-CNFs to translucency is very interesting. One possible explanation might be that the decomposition process such as fragmentation from single crystal and decrystallization to amorphous H-CNFs were involved in the change of structure and consequently imaging. We are going to study the change by experiment throughout the long term in the future.

H-CNFs in the subcutaneous tissue did not induce an acute severe inflammatory reaction. They were englobed by phagocytes such as macrophages and foreign body giant cells.

Acknowledgment. This work was supported by Health and Labor Sciences Research Grants in Research on Advanced Medical Technology in Nanomedicine Area from the Ministry of Health, Labor and Welfare of Japan.

References

(1) Mattson, M.; Haddon, R. C.; Rao, A. M. *J. Mol. Neurosci.* **2000**, *14*, 175.
(2) Elias, K. L.; Price, R. L.; Webster, T. J. *Biomaterials* **2002**, *23*, 3279.
(3) Price, R. L.; Waid, M. C.; Haberstroh, K. M.; Webster, T. J. *Biomaterials* **2003**, *24*, 1877.
(4) Nakamura, E.; Isobe, H. *Acc. Chem. Res.* **2003**, *36*, 807.
(5) McKenzie, J. L.; Waid, M. C.; Shi, R.; Webster, T. J. *Biomaterials* **2004**, *25*, 1309.
(6) Hu, H.; Ni, Y.; Montana, V.; Haddon, R. C.; Parpura, V. *Nano Lett.* **2004**, *4*, 507.
(7) Uo, M.; Akasaka, T.; Rosca, I.; Watari, F.; Yokoyama, A.; Omori, M.; Sato, Y.; Tohji, K. Abstract No 467; *205th Meeting of The Electrochemical Society*, meeting abstracts, MA 2004-01.
(8) Sato, Y.; Ohtsubo, M.; Shinoda, K.; Jeyadevan, B.; Tohji, K.; Motomiya, K.; Yamamoto, G.; Hashida, T.; Omori, M.; Yokoyama, A. Abstract No 584; *205th Meeting of The Electrochemical Society*, meeting abstracts, MA 2004-01.
(9) Yamago, S.; Tokuyama, H.; Nakamura, E.; Kikuchi, K.; Kananishi, S.; Sueki, K.; Nakahara, H.; Enomoto, S.; Ambe, F. *Chem. Biol.* **1995**, *2*, 385.
(10) Service, R. F. *Science* **1998**, *281*, 941.
(11) Huczko, A.; Lange, H.; Calko, E.; Grubek-Jaworska, H.; Droszez, P. *Fullerene Sci. Technol.* **2001**, *9*, 251.
(12) Huczko, A.; Lange, H. *Fullerene Sci. Technol.* **2001**, *9*, 247.
(13) Tamura, K.; Takashi, N.; Kumazawa, R.; Watari, F.; Totsuka, Y. *Mater. Trans.* **2002**, *43*, 3052.
(14) Kumazawa, R.; Watari, F.; Takashi, N.; Tanimura, Y.; Uo, M.; Totsuka, Y. *Biomaterials* **2002**, *23*, 3757.
(15) Service, R. F. *Science* **2003**, *300*, 243.
(16) Schvedova, A. A.; Castranova, V.; Kisin, E. R.; Schwegler-Berry, D.; Murray, A. R.; Gandelsman, V. Z.; Maynard, A.; Baron, P. J. *Toxicol. Environ. Health A* **2003**, *66*, 1909.
(17) Covin, V. L. *Nature Biotechnol.* **2003**, *21*, 1166.
(18) Maynard, A. D.; Baron, P. A.; Foley, M.; Schvedova, A. A.; Kisin, E. R.; Castranova, V. J. *Toxicol. Environ. Health A* **2004**, *67*, 87.
(19) Warheit, D. B.; Laurence, B. R.; Reed, K. L.; Roach, D. H.; Reynolds, G. A. M.; Webb, T. R. *Toxicol. Sci.* **2004**, 77, 117.
(20) Lam, C. W.; James, J. T.; McCuskey, R.; Hunter, R. L. *Toxicol. Sci.* **2004**, *77*, 126.
(21) Watari, F. *Abstract of Annual Meeting 2002 of Health and Labor Sciences Research Grants in Research on Advanced Medical Technology in Nanomedicine Area from the Ministry of Health, Labor and Welfare of Japan*, 2003.
(22) Fugetsu, B.; Satoh, S.; Iles, A.; Tanaka, K.; Nishi, N.; Watari, F. *Analyst* **2004**, *129*, 565.
(23) Sato, Y.; Jeyadevan, B.; Tohji, K.; Tamura, K.; Akasaka, T.; Uo, M.; Yokoyama, A.: Shibata, K.; Watari, F. *Abstract No. 4186; 206th Meeting of The Electrochemical Society*, meeting abstracts, MA 2004-02.
(24) Rodriguez, N. M. *J. Mater. Res.* **1993**, *8*, 3233.
(25) Rodriguez, N. M.; Chambers, A.; Baker, R. T. *Langmuir* **1995**, *11*, 3862.
(26) Jonas, L.; Fulda, G.; Radeck, C.; Henkel, K. O.; Holzhunter, G.; Mathieu, H. *J. Ultra Pathol.* **2001**, *25*, 375.
(27) Wang, J. C.; Yu, W. D.; Sandhu, H. S.; Betts, F.; Bhura, S.; Delamarter, R. B. *Spine* **2000**, *24*, 899.
(28) Liu, Z.; Ooi, K.; Kanoh, H.; Tang, W.; Tomida, T. *Langmuir* **2000**, *16*, 4154.
(29) Toomey, R.; Freidank, D.; Ruhe, J. *Macromolecules* **2004**, *37*, 882.
(30) Valberg, P. A.; Albertini, D. F. *J. Cell Biol.* **1985**, *101*, 130.

NL0484752

JOURNAL OF MATERIALS SCIENCE 38 (2003) 1039–1044

Influence of metal plating treatment on the electric response of Nafion

H. TAMAGAWA*, F. NOGATA*, T. WATANABE*, A. ABE*, K. YAGASAKI‡, J.-Y. JIN§
*Departments of *Human Information Systems, ‡Mechanical and Systems Engineering and §Chemistry, Faculty of Engineering, Gifu University, 1-1 Yanagido, Gifu-shi, Gifu-ken 501-1193, Japan*
E-mail: tmgwhrhs@cc.gifu-u.ac.jp

A potentially promising material as a high performance electroactive polymer gel actuator, Nafion, is known for its fast and large bending upon an applied voltage. Not long ago, it was reported that copper plating on Nafion enhances the degree of its bending. We performed the combinational metal plating treatment on Nafion surfaces with silver, copper and nickel, and the performances of metal plated Nafions—bending curvature and generated force—upon an applied voltage were quantitatively evaluated. From the obtained results, it was speculated that the hydrated mobile ions play substantial roles for the large bending of Nafion as has been widely believed and for the enhancement of its generated force. In addition to them, nickel plating on Nafion surfaces was found to enable Nafion to exhibit a large force without a significant force decay owing to the low-elastic property of nickel layers.

1. Introduction

Gel actuator has attracted researchers attention for the past decades [1–19]. Its expected soft motion, large shape change and low energy consumption by far exceed the conventional metal and ceramics actuators performance. Nafion is well-known material as the most promising future actuator material [9–15, 19]. It exhibits a relatively fast and large bending upon the low voltage as low as a few volts. The bending is reversible by the polarity change of applied voltage and this reversible bending can be continued thousands times. Some applications of Nafion actuator are a catheter, a dust wiper and etc. However, nobody has realized such Nafion products yet. Some of the difficulties lie in the occurrence of bending relaxation, the low generated force and the force decay.

Uchida and Taya reported that they successfully improved the bending performance of Nafion upon a voltage by forming copper layers on its surfaces [19]. We performed some experiments modifying their experiments, and investigated the bending curvature and the generated force of Nafion along with the current flowing through its body as a function of time. From the results obtained through these experiments, we could see a substantial role of mobile ions for the enhancement of bending. And we theoretically found a strong correlation of Nafion bending and its Young's modulus to the force it generates.

2. Experiment

2.1. Specimen preparation

Metal plating on the Nafion surfaces was performed, which primarily serves as a flexible electrodes on Nafion. Three different kinds of metal plating was applied on Nafions surfaces, silver, silver & copper and silver & copper & nickel.

2.1.1. Silver plated Nafion

Nafion surfaces were roughened with a sandpaper. The silver plating solutions, Solution-A and Solution-B, were prepared. Solution-A consists of silver nitrate (0.6 g), 5.0 N ammonium hydroxide (3.0 g) and deionized water (30.0 g). Solution-B consists of D-(+)-glucose (0.4 g), sodium hydroxide (0.8 g) and deionized water (20.0 g). A Nafion sheet was placed in Solution-A followed by the pouring of Solution-B. This process was repeated at least four times to do the better plating on Nafion surface. Silver nitrate and ammonium hydroxide were purchased from Aldrich (Miwaukee, WI). D-(+)-glucose and sodium hydroxide were purchased from NACALAI TESQUE, Inc. (Kyoto, Japan).

The silver plated Nafion sheet was cut into the strips, 20 mm-length × 1 mm-width and dried in the atmosphere for 1 day. Then they were immersed in two different solvents, deionized water and 0.1 M HCl aqueous solution for a day. Nafion swollen with deionized water and 0.1 M HCl were was designated as N-DIW and N-H, respectively.

2.1.2. Silver & copper plated Nafion

First, N-DIW was prepared, and it was plated with copper by following procedure. Copper plating solution consists of copper (II) sulfate pentahydrate (20.0 g), sulfiic acid (7.5 g) and deionized water (100.0 g). Nafion

0022–2461

and a small piece of a copper plate connected to the power supply were placed in the copper plating solution, and 1 A-current and 3 V-voltage was applied for 3 s. This plated Nafion piece was cut into the strips, 20 mm-length × 1 mm-width. It was designated as N-SC. Copper (II) sulfate pentahydrate was purchased from Aldrich (Miwaukee, WI). Sulfic acid was purchased from Wako Pure Chemical Industries, Ltd. (Osaka, Japan).

2.1.3. Silver & copper & nickel plated Nafion

First, N-SC was prepared, and immediately nickel plating was performed on its surfaces. Nickel plating solution consists of nickel (II) sulfate hexahydrate (15.0 g), ammonium chloride (1.5 g), boric acid (1.5 g) and deionized water (100.0 g). Nafion and a nickel wire connected to the power supply were placed in the copper plating solution, and 2 A-current and 7 V-voltage was applied for 7 s. This plated Nafion piece was cut into the strips. It was designated as N-SCN. All chemicals were purchased from Wako Pure Chemical Industries, Ltd. (Osaka, Japan).

2.2. Measurement

2.2.1. Bending curvature and current of Nafion

The curvature of all Nafion specimens was measured upon 1 V, as a function of time using an experimental setup depicted in Fig. 1, where Nafion was in the free bending state.

2.2.2. Force and current of Nafion

The force generated by Nafion bending upon 1 V, was measured as a function of time using an experimental setup depicted in Fig. 2. Nafion strip was placed on the fixture attached on the jack. The tip of Nafion was placed on the balance. The force generated by this bending Nafion was measured with this balance, where Nafion length excluding a part of it grabbed by the fixture was 15 mm. As is obvious, the downward movement of Nafion tip is restrained by the balance, namely, Nafion is in the restraint bending state.

2.2.3. Young's modulus of Nafion

Young's modulus of Nafion was obtained. Fig. 3 is an experimental setup. A straight shape Nafion strip was

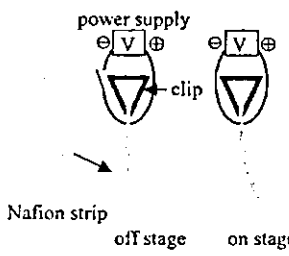

Figure 1 Experimental setup for the measurement of Nafion curvature.

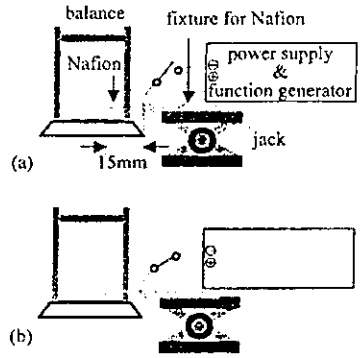

Figure 2 Experimental setup for the measurement of generated force of Nafion: (a) No generated force because of no bending of Nafion upon 0(V) and (b) Occurrence of force generation by Nafion bending upon applied voltage.

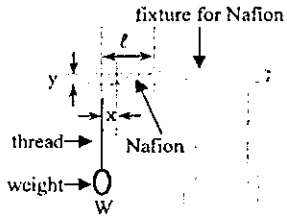

Figure 3 Experimental setup for the measurement of Young's modulus of Nafion. W, E and ℓ are the force exerted on the tip of Nafion, Young's modulus of Nafion, and the length of straighten Nafion, respectively.

placed on the fixture. On the tip of Nafion, a thread with a small weight (W) was attached. Nafion bent due to this weight, and the coordinate values of this bent Nafion (x, y) defined as in Fig. 3 were obtained experimentally. The coordinate values of Nafion have a relationship with W represented by Equation 1.

$$y = W(x^3 - 3\ell^2 x + 2\ell^3)/6EI \qquad (1)$$

where E, I and ℓ are Young's modulus, the moment of inertia of cross section, and the length of Nafion in the straight shape, respectively. I is defined by $I = bh^3/12$ where b and h are the width and thickness of Nafion specimen, respectively. Since all the values in Equation 1 except for E can be easily obtained experimentally, E can be calculated.

3. Results and discussions

3.1. Bending curvature and current of Nafion

Fig. 4 shows time dependence of curvature of Nafion specimens upon 1 V, where the positive value of curvature is defined as the bending toward positive electrode direction. All Nafion specimens but N-SCN exhibit quite large bending curvatures immediately after starting imposing a voltage. Especially N-H exhibits an extremely large bending, but it's followed by a large bending relaxation. It's a big issue to be overcome for the purpose of making Nafion actuator.

The bending of Nafion is widely believed to be caused by the shift of hydrated mobile ions contained in its body [9, 15, 19]. If such a concept is right, even a

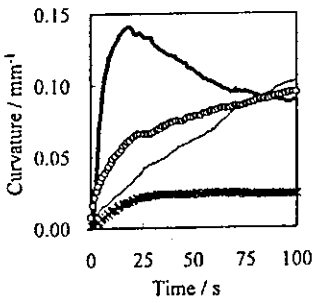

Figure 4 Time dependence of Nafion curvature upon 1 V where the positive value of curvature is defined as the bending of Nafion toward the positive electrode direction. Thin line, fat line, circle, and × mark represent the data of N-DIW, N-H, N-SC, and N-SCN, respectively.

neutral membrane could be bent upon a voltage, when it contains an ionic solution. We performed a following experiment: A neutral dialysis membrane was plated with silver and immersed in the copper plating solution prepared following the description in Section 2.1.2 in order to import mobile ions in it. This dialysis membrane exhibited a bending upon 1 V. Therefore almost undoubtedly the mobile hydrated ions contained in N-DIW, N-H, N-SC, and N-SCN, play a dominant role for the bending. However, the exact mechanism of their bending could not be elucidated fully. Then we performed additional investigations described below, and we'll show our speculations on the cause of these Nafions bending along with our finding obtained from those investigations.

We prepared N-DIW, N-H, N-SC, and N-SN, where N-SN was prepared simply by skipping a copper plating process for N-SCN detailed in Section 2.1.3. Using an experimental setup depicted in Fig. 1, we performed curvature and current measurement for them, where the applied voltage was monotonously raised as given by Equation 2.

$$V(t) = 10\,(\mathrm{mV/s}) \cdot t(\mathrm{s}) \qquad (2)$$

where V and t represent the applied voltage and time, respectively.

Time dependences of the current flowing through Nafion and of their curvature are shown in Fig. 5a and b, respectively. We have to make some comments on this experiment on N-SC as next. The smaller specimens of N-SC were used for the measurement of current, since its value is extremely high out of range of our equipment. Therefore the value of current using a normal size of N-SC is expected to be quite higher than that in Fig. 5a.

Current of all Nafion specimens abruptly increase before reaching $t = 25$(s), and the curvature of them but N-SN exhibit abrupt increase, too, correspondingly. It's in line with the concept of the occurrence of shift of hydrated mobile ions as a cause of Nafion bending. Since all of them have H^+ as mobile ions in common, their bending except for N-SN is speculated to be due to the shift of hydrated H^+. And the extremely large bending of N-H must be due to the import of H^+ through the immersion of it in 0.1 M HCl solution in its preparation

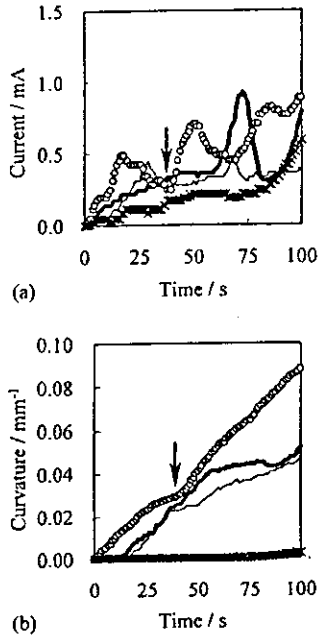

Figure 5 Time dependence of Nafion current and curvature upon $V(t) = 10(\mathrm{mV}) \cdot t(\mathrm{s})$ where thin line, fat line, circle, and × mark represent the data of N-DIW, N-H, N-SC, and N-SN, respectively. (a) Current and (b) curvature.

stage. The cause of no bending of N-SN is explained in the latter part of this section.

The current of N-SC exhibits a quite unique behavior, it has three current peaks. Especially the onset point of second current peak indicated by an arrow in Fig. 5a attracted our attention, where the applied voltage at this onset point is around 0.35 (V). At the very same moment, a discontinuous bending indicated by an arrow in Fig. 5b was observed. This must be due to the occurrence of the reaction $Cu^{2+} + 2e^- \rightarrow Cu$. Namely, N-SC was doped with Cu^{2+} during the copper plating stage. Doped Cu^{2+} ion got hydrated in N-SC and continuously transferred to the negative side around at 0.35 (V). They were converted into Cu atoms by receiving two electrons at the negative side. This reaction process must cause the discontinuous bending as in Fig. 5b. As a matter of fact, it has been already widely known that the reaction $Cu^{2+} + 2e^- = Cu$ occurs at $V = 0.337$(V) (vs NHE) [20]. Since 0.337(V) for the occurrence of $Cu^{2+} + 2e^- \rightarrow Cu$ is measured against NHE, one may say that it is not right to claim that this reaction occurs in N-SC. However, this reaction appears to be even visible in a certain condition as described next. A silver plated Nafion containing copper plating solution was prepared. We observed the color change of its negative surface into red around upon 0.35 (V). This red color must be the color of reduced Cu created by the reaction $Cu^{2+} + 2e^- \rightarrow Cu$. So this reaction must occur to N-SC, too, around at $V = 0.35$ (V), although it is invisible for N-SC due to its originally dark color. Cu^{2+} can be regarded as a strong promoter for the Nafion bending. Here we add some words on this phenomenon. The enhancement of bending of copper plated Nafion, N-SC, must be primarily due to Cu^{2+} doped into N-SC rather

than Cu^{2+} created from copper layer on N-SC. Detail analysis on it is explained in reference [21] written by some of the authors of this pape.

Up to $V = 0.75$(V), virtually no bending was observed for N-SN. Since it exhibits a considerable value of current as in Fig. 5(a), it must contain some mobile ions such as H^+ and Ni^{2+} and etc, where Ni^{2+} was doped into N-SC through the nickel plating treatment. Occurrence of no bending must be due to the large stiffness of N-SN by the nickel plating. Nickel layers on N-SN are quite stiff. Therefore a not-quite-yet-relatively-large bending observed for N-SCN stiffened with nickel layers shown in Fig. 4 must be primarily owing to existence of Cu^{2+} in its body, which leads to the occurrence of reaction $Cu^{2+} + 2e^- \rightarrow Cu$ as described above and cause a bending.

Around above $V = 0.75$(V), all the Nafion specimens including even N-SN exhibit bending. The current behavior corresponding to their bending behavior at this voltage region is quite complicated, and hard to identify what's going on. Yet, Ag^+ must also come to play a role for the bending along with H^+, or H^+ and Cu^{2+} to some extent. All the Nafion specimens have silver layers on their surfaces, and it's been widely known that the reaction of $Ag^+ + e^- = Ag$ occurs at 0.799(V) (vs NHE) [20]. Namely, Ag on the positive surface is ionized into Ag^+ and hydrated at this voltage region. Then it is transferred to the negative side and converted into Ag atoms by receiving one electron. This process must be continuously occurring, resulting in the bending. Although 0.799(V) for the reaction $Ag^+ + e^- = Ag$ is measured against NHE, the reaction $Ag \rightarrow Ag^+ + e^-$ is strongly speculated to occur in Nafion, since $Cu^{2+} + 2e^- \rightarrow Cu$ also appears to occur in Nafion at the close voltage against NHE as described earlier.

3.2. Force, current, and Young's modulus of Nafion

Even though Nafion can exhibit a large bending in the free bending state as in Fig. 4, it's not worth using as an actuator material, unless it generates a large enough force and exhibits no force decay as well as exhibits a relatively large bending. Time dependence of force generated by Nafion specimens upon 1 V is shown in Fig. 6, where it was measured by using

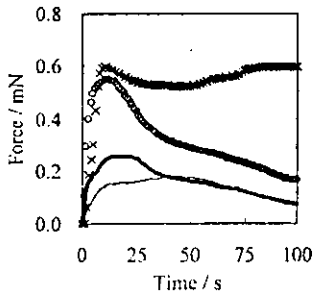

Figure 6 Time dependence of force generated by Nafion upon 1 V where thin line, fat line, circle, and × mark represent the data of N-DIW, N-H, N-SC, and N-SCN, respectively.

TABLE I Young's modulus (E) of Nafion

	N-DIW	N-H	N-SC	N-SCN
E (GPa)	0.09	0.12	0.14	1.24

an experimental setup depicted in Fig. 2. N-SC and N-SCN generate quite large force. Especially, N-SCN did not exhibit a force decay, while N-SC exhibited. It is an attractive facet of N-SCN, yet a long duration time of applied voltage results in the uncontrollability on its force.

As described earlier, the bending of N-SCN is not so large as that of the other even in the free bending state as in Fig. 4, although it exhibited a quite large force as in Fig. 6. Therefore the enhancement of bending is not a sole cause of the generation of large force. There should exist another cause of large force. The most likely cause of large generated force of N-SCN is its large stiffness. Young's modulus of Nafion measured using an experimental setup depicted in Fig. 3 is summarized in Table I. While the bending curvature of N-SCN is far smaller than those of N-DIW or N-H, its Young's modulus is obviously far larger than N-DIW and N-H. Therefore stiffer matrix of N-SCN must play a role of enhancement of its generated force.

Here we discuss the relationship among the force (f), Young's modulus (E), and the bending moment (M_0) of Nafion theoretically. Three of the authors of this paper have proposed a simple evaluation method for the dynamic behavior of Young's modulus of Nafion in the restraint bending state as depicted in Fig. 2 [22]. The theoretical part of it is described next. Fig. 7 is a model of Nafion in the restraint bending state. In this model, the bending of Nafion is assumed to be small, and the vertical force exerted to the tip of Nafion in the process of bending is assumed to be the same as the force, f, generated by Nafion.

$$EI(d^3y/dx^3) + [f - \rho g(\ell - s)] = 0 \qquad (3)$$

ρ, g, ℓ, and I are the mass per unit length of Nafion, gravitational acceleration, the length of Nafion, and the moment of inertia of cross section of Nafion, respectively.

Under the boundary conditions, $y(0) = 0$, and $(dy/dx)(0) = 0$, Equation 4 is obtained from Equation 3.

$$y = -[(f - \rho g\ell)x^3/6 + \rho g x^4/24 + Cx^2]/EI \qquad (4)$$
$$C = \text{const}$$

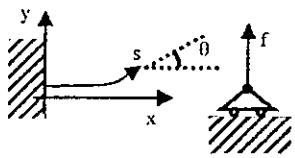

Figure 7 A model of Nafion exerting a force in the process of self-bending upon applied voltage.

Since $y(\ell) = 0$, $y'(\ell) = -\alpha$, and $M_o = EI\alpha$, Equation 5 is obtained from Equation 4, where α is the curvature of Nafion.

$$f = 6M_o/\ell^2 + \rho g\ell/2 = 6EI\alpha/\ell^2 + \rho g\ell/2 \quad (5)$$

Equation 5 suggests that the force of Nafion has a strong correlation to its Young's modulus and curvature. Even though the bending curvature of Nafion is quite small, the large Young's modulus can make up for it. It agrees with the observation of a large force by N-SCN that is less deformable than N-SC. Another thing, the force depends merely on the bending moment (M_o). Since the maximum forces of N-DIW and N-H are close each other and those of N-SC and N-SCN are almost the same each other, the maximum bending moments of N-DIW and N-H are speculated to be close each other and those of N-SC and N-SCN are speculated to be almost the same.

Since the validity of this theory is limited to the elastic small bending of Nafion [21], it cannot apply to the whole bending behaviors of Nafions. However, the early stage of Nafion bending is speculated to be dominated by the elastic deformation from our observations. Therefore this theory is valid at least in the early bending stage till we can observe the fast increase of curvature as in Fig. 4 and the sharp increase of force as in Fig. 6.

In order to see in detail what's going on in their force generation process of Nafion, we performed force and current measurement for N-DIW, N-H, N-SC, and N-SN, where the applied voltage is given by Equation 2. The results are shown in Fig. 8, where we have to bear in mind that the size of N-SC specimen was intentionally made smaller than normal size due to the same reason described in Section 3.1. However, even small specimens of N-SC exhibit large current out of range of our equipment, yet a few of them exhibit small enough current. We intentionally chose such data of small current and corresponding generated force. Therefore concerning N-SC, we can discuss only the trend of current and force behaviors and cannot discuss their values.

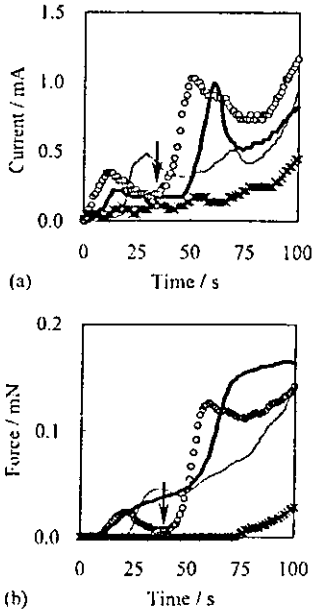

Figure 8 Time dependence of current and force by Nafion upon $V(t) = 10\,(\mathrm{mV}) \cdot t\,(\mathrm{s})$ where thin line, fat line, circle, and × mark represent the data of N-DIW, N-H, N-SC, and N-SN, respectively. (a) Current and (b) force.

Making comparison of Fig. 8a and b, we can observe unambiguously a direct correlation between the current and force. Abrupt increase of generated force is mostly observed at the moment when abruptly current increases. It suggests that shift of mobile hydrated ions enhances the force generation. The current of N-SC again attracts our attention, especially at the onset point of its second peak of current, its force also abruptly starts increasing, where both indicated by arrows in Fig. 8a and b, respectively. This must be due to the reaction of $Cu^{2+} + 2e^- \rightarrow Cu$.

N-SN did not exhibit a large force as in Fig. 8b, although it was stiffened with nickel layers, which suggests that N-SN tended to bend only to a slight degree. On the other hand, N-SCN exhibits a quite large force as in Fig. 6, which suggests that N-SCN tended to bend more largely than N-SN. From these observations, it is speculated that the large force by N-SCN is due to the strong tendency of bending by the shift of primarily hydrated Cu^{2+} upon applied voltage along with its stiffened matrix, which agrees with our speculation on the cause of free bending of N-SCN described in Section 3.1.

One may think that simply extending the duration time of copper plating for N-SC beyond 3 s could bring us another type of N-SC which is well stiffened with thicker copper layers and highly doped with Cu^{2+}. Such N-SC is expected to exhibit a more effective bending and generate a larger force. In order to answer this question, a copper plated Nafion was prepared by extending the copper plating time of N-SC up to 9 s, three times as long as a normal N-SC, and the time dependence of its curvature and force upon I(V) was measured, where this specimen was designated as N-SC3. The results are shown in Fig. 9. We could not see any improvement on the bending curvature or the generated force, compared with those of N-SC in Figs 4 and 6, respectively. Furthermore, the copper plating layer is not stable enough unlike a nickel plating layer. It easily comes off the N-SC surfaces. However, doping itself is important for the effective bending of Nafion, since its bending is strongly speculated to be dominated by the mobile hydrated ions contained in it as described earlier. For instance, N-S immersed in the copper plating solution for a day absorbs a large amount of Cu^{2+} and bends largely extremely upon I(V). But N-SC3 does not appear to be doped more than N-SC judging from the results on its force curvature behaviors. Probably the thicker copper layer on N-SC3 prevents the heavy doping.

Additional thing, there appears to be a trend difference in the current of Nafions between in the free bending and in the restraint bending states especially as for

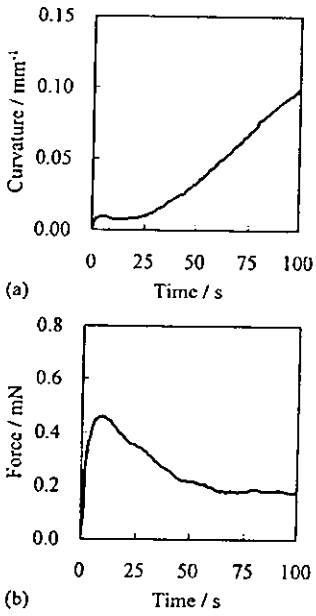

Figure 9 Time dependence of curvature and force by N-SC3 upon 1 V. (a) Curvature and (b) force.

N-SC. Figs 5a and 8a show the current of Nafions in the free bending and in the restraint bending states, respectively. Although we cannot make a direct comparison of the absolute values of current of N-SC because of the reduction of their size and etc, obviously their trend is different each other. The current behavior of Nafion might be quite susceptible to the external force and the degree of its bending. It demands a further investigation in detail.

4. Conclusion

The fundamental properties for the actuator—a relatively large bending and generated force—were given to Nafion through the combination of metal plating with silver, copper, and nickel. It gives Nafion an additional benefit—no force decay. However, we found another problem of N-SCN—uncontrollability of its bending. Overcoming this uncontrollability is one of the important next tasks for us.

Acknowledgment

This research was conducted under the supports of Gifu Daigaku Kasseika Kenkyuuhi (Gifu University research promotion fund) and Health and Labour Sciences Research Grants from Ministry of Health Labour and Welfare, Japan. We'd like to express our gratitude to Nihon Polymer (Kasugai, Aichi, Japan) for providing us with Nafion sheets.

References

1. T. TANAKA, I. NISHIO, S.-T. SUN and S. UENO-NISHIO, *Science* **218** (1982) 467.
2. T. SHIGA, Y. HIROSE, A. OKADA and T. KURAUCHI, *Kouhunshironbunshu* **46** (1989) 709.
3. T. SHIGA and T. KURAUCHI, *J. Appl. Poly. Sci.* **39** (1990) 2305.
4. S. UMEMOTO, T. MATSUMURA, T. SAKAI and N. OKUI, *Polymer Gels and Networks* **1** (1993) 115.
5. T. HIRAI, H. NEMOTO, M. HIRAI and S. HAYASHI, *J. Appl. Polym. Sci.* **53** (1994) 79.
6. T. SHIGA, Y. HIROSE, A. OKADA and T. KURAUCHI, *J. Mater. Sci.* **29** (1994) 5715.
7. M. HIRAI, T. HIRAI, A. SUKUMODA, H. NEMOTO, Y. AMEMIYA, K. KOBAYASHI and T. UEKI, *J. Chem. Soc. Faraday Trans.* **91** (1995) 473.
8. K. SALEHPOOR, M. SHAHINPOOR and M. MOJARRAD, in Proceedings of SPIE Smart Materials and Structures, San Diego, 1996, Vol. 2716, p. 116.
9. K. ASAKA, K. OGURO, Y. NISHIMURA, M. MIZUHARA and H. TAKENAKA, *Polym. J.* **27** (1995) 436.
10. R. KANNO, S. TADOKORO, T. TAKAMORI and M. HATTORI, in Proceedings of the 1996 IEEE International Conference on Robotics and Automation, Minneapolis, 1996, p. 219.
11. K. SALEHPOOR, M. SHAHINPOOR and M. MOJARRAD, in Proceedings of SPIE Smart Materials and Structures, San Diego, 1997, Vol. 3040, p. 192
12. M. SHAHINPOOR, M. MOJARRAD and K. SALEHPOOR, in Proceedings of SPIE Smart Materials and Structures, San Diego, 1997, Vol. 3041, p. 829.
13. Y. BAR-COHEN, T. XUE, M. SHAHINPOOR, K. SALEHPOOR, J. SIMPSON, J. SMITH and P. WILLIS, in Proceedings of SPIE Smart Materials and Structures, San Diego, 1998, Vol. 3324, p. 218.
14. M. SHAHINPOOR, Y. BAR-COHEN, T. XUE, J. SIMPSON and J. SMITH, in Proceedings of SPIE Smart Materials and Structures, San Diego, 1998, Vol. 3324, p. 251.
15. K. OGURO, K. FUJISAWA, K. ASAKA, K. ONISHI and S. SEWA, in Proceedings of SPIE Smart Materials and Structures, San Diego, 1999, Vol. 3669, p. 64.
16. T. HIRAI, J. ZHENG and M. WATANABE, in Proceedings of SPIE Smart Materials and Structures, San Diego, 1999, Vol. 3669, p. 209.
17. H. TAMAGAWA, S. POPOVIC and M. TAYA, in Proceedings of Materials Research Society Symposium Electroactive Polymers (EAP), Boston, 2000, Vol. 600, p. 273.
18. H. TAMAGAWA, S. POPOVIC and M. TAYA, *Polymer* **41** (2000) 7201.
19. M. UCHIDA and M. TAYA, *ibid.* **42** (2001) 9281.
20. T. OOSAKA, I. K. KANOU and S. KUWABATA, in "Beisikku Denkikagaku" (Basic Electrochemistry) (Kagakudoujin, Kyoko, 2000) p. 189 (in Japanese).
21. H. TAMAGAWA, F. NOGATA, T. WATANABE, A. ABE and K. YAGASAKI, in Proceedings of IEEE ICIT'02, Bangkok, 2002.
22. H. TAMAGAWA, K. YAGASAKI and F. NOGATA, *J. Appl. Phys.*, accepted.

Received 5 October 2001
and accepted 5 November 2002

Available online at www.sciencedirect.com
SCIENCE DIRECT
Journal of Colloid and Interface Science 275 (2004) 113–122
JOURNAL OF Colloid and Interface Science
www.elsevier.com/locate/jcis

Extension of Colacicco's experiment supporting the adsorption theory

Hirohisa Tamagawa * and Fumio Nogata

Department of Human and Information Systems, Faculty of Engineering, Gifu University, 1-1 Yanagido, Gifu 501-1193, Japan

Received 23 September 2003; accepted 20 January 2004
Available online 6 March 2004

Abstract

The pervasive concept of the cause of the potential occurring across a semipermeable membrane intervening between two ionic solutions is called the membrane theory; hence, this potential is called the membrane potential. Although almost nobody has doubted its validity, research results defying it have been continuously reported by a small number of researchers. They have claimed that the cause the potential lies in the adsorption of ions onto adsorption sites, which is the adsorption theory. One such research report by G. Colacicco (Nature 207 (1965) 936) was employed for our experimental work reported in this paper in order to examine the validity of the membrane theory and the adsorption theory. The results we obtained are in conflict with the membrane theory but appear to be in full agreement with the long dismissed adsorption theory. This paper urges the reexamination of the membrane theory and the reconsideration of the adsorption theory from a nonbiased standpoint.

Keywords: Membrane theory; Nernst equation; Hodgkin–Katz–Goldman equation; Adsorption theory

1. Introduction

The membrane theory has for a long while been accepted as a fully established concept for the prediction of potential behavior generated between two ionic solutions separated by a semipermeable membrane [1–8]. Indeed, its successful use is often visible. A large number of papers, textbooks, technical books, small explanatory articles, etc. have been readily at hand. Although the membrane theory is seemingly categorized in electrochemistry or physical chemistry [9], namely, it seems to have meaning only for pure science in the laboratory, it has profound meaning for our life. The membrane theory accounts for a large part of physiology [2,4–8], called electrophysiology. The function of the nervous system in the human body has been analyzed primarily based on the membrane theory, and it is reduced to actual benefits for our own life. So the membrane theory has a strong connection to us. Therefore, deepening the understanding of the membrane theory even more must be quite profitable. However, some people have denied the membrane theory [1–5,7,8,10–12], and they have advocated an alternative theory, the adsorption theory. They say that the potential generation across the semipermeable membrane is caused not by the selective permeability of the membrane, as the membrane theory predicts, but by ion adsorption onto the adsorption site existing on the membrane surface. According to their claim, there are countless counterexamples to the membrane theory that are in full agreement with the adsorption theory. However, they have all been dismissed for decades, while a great number of evidences in line with the membrane theory alone have attracted strong attention [2,4,5,7,8]. Although the adsorption theory has been out of researchers' attention nowadays, a reconsideration of it provokes the thought to us that the adsorption theory even has aspects superior to the membrane theory in explain potential behavior across semipermeable membranes.

In this work, we modified experimental work performed by Colacicco [1], which denies the membrane theory and validates the adsorption theory, into a more generalized one and examined the validity of the membrane theory again. We suggest the necessity of reconsideration of the adsorption theory.

2. Methods and materials

Basically we followed the Colacicco procedure [1]. Two compartments containing ionic solutions are contacted with

* Corresponding author.
E-mail address: tmgwhrhs@cc.gifu-u.ac.jp (H. Tamagawa).

0021-9797/$ – see front matter
doi:10.1016/j.jcis.2004.01.038

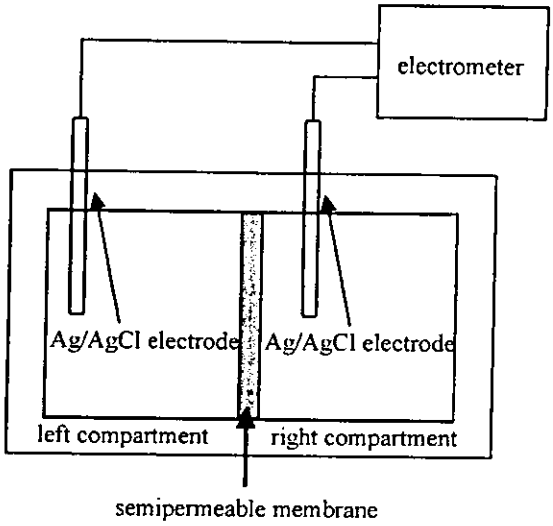

Fig. 1. The apparatus employed for the measurement of the potential generated by two ionic solutions separated by a semipermeable membrane.

each other through the intermediary of a semipermeable membrane. We employed a number of different species and concentrations of ionic solutions to fill the compartments, and we also employed several different membranes as semipermeable membranes separating two ionic solutions in the compartments. We measured the potential across the membrane by inserting Ag/AgCl electrodes into each compartment and examined the potential behavior, where all the potential measurements were performed at room temperature.

3. Results and discussion

3.1. Potential across neutral, anionic, and cationic membranes

Employing the apparatus depicted in Fig. 1, the potential generated by two ionic solutions separated by a semipermeable polymer membrane was measured, where the potential, V_{exp}, was defined by V_{exp} = (potential of the right compartment) − (potential of the left compartment) for the whole potential measurements described in this paper unless additional comments are given. We employed three different types of semipermeable polymer membranes, dialysis membrane, Nafion (DuPont, DE, USA), and Selemion (Asahi Glass Co., Tokyo, Japan). Dialysis membrane is a neutral membrane, and Nafion is a negatively charged membrane. For Selemion, we used a positively charged membrane, although both negatively and positively charged Selemion are commercially available.

Tables 1–3 show the measured potential along with the type and the concentration of ionic solutions supplied in the left and right compartments of the experimental apparatus. These potential behaviors are normally explained by the membrane theory—the Nernst equation or its generalized expression, the Hodgkin–Katz–Goldman equation

Table 1
The potential across dialysis membrane

Notation	Left solution	Right solution	V_{exp} [mV]	V_{cal} [mV]
d1	0.01 M KCl	0.10 M KCl	−4	0
d2	0.05 M KCl	0.10 M KCl	−4	0
d3	0.10 M KCl	0.10 M KCl	−3	0

Notes. Left solution ≡ the type of solution and its concentration in the left compartment. Right solution ≡ the type of solution and its concentration in the right compartment. V_{exp} ≡ the experimentally measured potential across the dialysis membrane. V_{cal} ≡ the theoretically calculated potential across dialysis membrane based on the membrane theory, assuming the dialysis membrane is quite permeable to K^+ and Cl^-.

(HKG equation) [2,4,8]. First, we try to explain these potential behaviors employing the HKG equation of the membrane theory as below.

3.1.1. Potential across the dialysis membrane

The potentials of d1, d2, and d3 in Table 1 are explained employing the HKG equation:

$$V = (RT/F)\ln\left[\left(\sum_i P_{a_i^+}[a_i^+]_l + \sum_j P_{a_j^-}[a_j^-]_r\right) \Big/ \left(\sum_m P_{a_m^+}[a_m^+]_r + \sum_n P_{a_n^-}[a_n^-]_l\right)\right]. \quad (1)$$

R, T, and F are the gas constant, the absolute temperature, and the Faraday constant, respectively. $[a_\alpha^+]_\beta$ and $[a_\alpha^-]_\beta$ are the activity of the cation of a_α^+ and of the anion of a_α^-, respectively, where β ($= l$ and r) denotes the left compartment and the right compartment, respectively. $P_{a_\alpha^+}$ and $P_{a_\alpha^-}$ are the permeability constants of a_α^+ and a_α^- through the membrane, respectively.

This equation is, for instance, applied to d1, giving the theoretically calculated potential, V_{cal}, where V_{cal} of d1 is expressed by $V_{cal}(d1)$, and hereafter the way of this expression is employed for the representation of the potential:

$$V_{cal}(d1) = (RT/F)\ln\left[\left(P_{K^+}[K^+]_l + P_{Cl^-}[Cl^-]_r\right) \Big/ \left(P_{K^+}[K^+]_r + P_{Cl^-}[Cl^-]_l\right)\right]. \quad (2)$$

If K^+ and Cl^- both can permeate freely through the dialysis membrane, that is, the dialysis membrane does not have selective permeability, Eq. (2) is reduced to

$$V_{cal}(d1) = (RT/F)\ln\left[\left([K^+]_l + [Cl^-]_r\right) \Big/ \left([K^+]_r + [Cl^-]_l\right)\right]. \quad (3)$$

Actually, we observed no osmotic pressure across the dialysis membrane. Therefore Eq. (3) is validated. From Eq. (3), $V_{cal}(d1) = 0$ mV, which is close to the experimentally measured potential of d1, $V_{exp}(d1)$, given in Table 1. Application of the same argument to d2 and d3 results in $V_{cal}(d2) = 0$ mV and $V_{cal}(d3) = 0$ mV, where these values are shown in Table 1, too. As to the potential across the dialysis membrane, we could see good agreement between V_{exp} and V_{cal}. This suggests the validity of the membrane theory.

Table 2
The potential across Nafion

Notation	Left solution	Right solution	V_{exp} [mV]	V_{cal} [mV]
n1	0.10 M KCl	0.10 M KCl	0	0
n2	0.10 M NaCl	0.10 M NaCl	0	0
n3	0.10 M KCl	0.05 M KCl	+17	+18
n4	0.10 M KBr	0.10 M KI	+1	0
n5	0.10 M NaBr	0.10 M NaI	+2	0
n6	0.10 M KI	0.10 M NaI	+9	–
n7	0.10 M KBr	0.10 M NaBr	+9	–
n8	0.10 M NaCl: 0.10 M NaI = 1:1 in vol	0.10 M NaCl	0	0
n9	0.10 M KCl:0.10 M KI = 1:1 in vol	0.10 M KCl	+1	0
n10	0.10 M KCl	0.05 M $CaCl_2$	+10	–
n11	0.05 M $CaCl_2$	0.05 M $FeCl_2$	+18	–

Notes. Left solution ≡ the type of solution and its concentration in the left compartment. Right solution ≡ the type of solution and its concentration in the right compartment. V_{exp} ≡ the experimentally measured potential across Nafion. V_{cal} ≡ the theoretically calculated potential across Nafion based on the membrane theory assuming it is quite permeable to cations and quite impermeable to anions. The left solutions of n8 and n9 are a mixture of 0.10 M NaCl and 0.10 M NaI at a 1:1 volume ratio and a mixture of 0.10 M KCl and 0.10 M KI at a 1:1 volume ratio, respectively.

3.1.2. *Potential across Nafion*

Employing the HKG equation, we can calculate the potentials of n1–n11 as in Table 2. The potentials of n1 and n2 are theoretically calculated. We do not need to know the values of the permeability constants, since the same species and concentrations of ions are in both left and right compartments. The results are given as V_{cal} in Table 2. V_{cal} of n1 and n2 are the same as V_{exp} of them.

The experimentally obtained potentials of n3, n4, and n5 can be obtained through HKG equation, too, under a certain assumption. Nafion contains a fixed anionic group; namely, it is a negatively charged membrane. Therefore the negatively charged particles, anions, are speculated to hardly permeate through Nafion compared with the positively charged particles, cations. This speculation is interpreted as $P_{K^+} \gg P_{Cl^-}$ in case HKG equation is applied to n3. Hence, Eq. (1) is transformed into

$$V_{cal}(n3) = (RT/F)\ln\big[\big(P_{K^+}[K^+]_l + P_{I^-}[Cl^-]_r\big) \big/ \big(P_{K^+}[K^+]_r + P_{Cl^-}[Cl^-]_l\big)\big] \approx (RT/F)\ln\big[[K^+]_l/[K^+]_r\big]. \quad (4)$$

Since the potential measurement was performed within a few minutes after the completion of setting up the experimental apparatus depicted in Fig. 1, $[K^+]_l$ and $[K^+]_r$ did not seem to change greatly from their initial concentrations. Therefore $[K^+]_l \approx 0.10$ M and $[K^+]_r \approx 0.05$ M. This gives $V_{cal}(n3) = +18$ mV, which is quite close to $V_{exp}(n3) = +17$ mV.

Applying the same argument to n4 and n5 results in the same type of equation as Eq. (4), and V_{cal} of n4 and n5 is 0 mV for both. This is quite close to V_{exp} of n4 and n5.

The same arguments applied to n3, n4, and n5 are applied to n6, too, resulting in

$$V_{cal}(n6) = (RT/F)\ln\big[\big(P_{K^+}[K^+]_l + P_{Na^+}[Na^+]_l + P_{I^-}[I^-]_r\big) \big/ \big(P_{K^+}[K^+]_r + P_{Na^+}[Na^+]_r + P_{I^-}[I^-]_l\big)\big]. \quad (5)$$

We can immediately derive the relationship of $P_{K^+}, P_{Na^+} \gg P_{I^-}$ as to the permeability constants. Under this condition, Eq. (5) is reduced to

$$V_{cal}(n6) \approx (RT/F)\ln\big[\big(P_{K^+}[K^+]_l + P_{Na^+}[Na^+]_l\big) \big/ \big(P_{K^+}[K^+]_r + P_{Na^+}[Na^+]_r\big)\big]. \quad (6)$$

Since we do not know the values of P_{K^+} and P_{Na^+}, we cannot proceed with their further calculation. We cannot obtain the theoretical value of $V_{cal}(n6)$. But we can speculate that P_{K^+} and P_{Na^+} are different from each other, which might cause the nonzero potential of $V_{exp}(n6) = +9$ mV in Table 2. The same argument is applicable to explain the nonzero potential of n7. Namely, each ionic species is speculated to have its own permeability constant, resulting in the nonzero potential, and that is what the HKG equation is based on.

The experimentally measured potentials of n8 and n9 are the same as or quite close to 0 mV; we can virtually see them as 0 mV, although the ionic species of the right compartment of n8 and n9 are different from those of the left compartment. Considering the argument so far, we can speculate that the cations play the predominant role in the determination of potential behavior. Taking up n8, the cation species and its concentration in both left and right compartments are exactly the same, Na^+ of 0.10 M. With these facts in mind, we can derive

$$V_{cal}(n8) \approx (RT/F)\ln\big[[Na^+]_l/[Na^+]_r\big]. \quad (7)$$

Since the potential measurement was performed within a few minutes after the completion of setting up the experimental apparatus depicted in Fig. 1, $[Na^+]_l$ and $[Na^+]_r$ did not seem to change greatly from their initial concentrations. Thus $V_{cal}(n8) \approx 0$ mV, which agrees with $V_{exp}(n8) = 0$ mV. The same argument is applicable to n9, too.

V_{cal} of n10 and n11 cannot be obtained theoretically for the same reason as the potential of n6 and n7. But their nonzero potentials are strongly speculated to be due to the difference of the values among P_{K^+}, $P_{Ca^{2+}}$, and $P_{Fe^{2+}}$.

3.1.3. *Potential across Selemion*

For the explanation of potentials of s1–s11, basically the same argument to n1–n11 are applicable.

Employing the HKG equation, we can calculate the potential of s1 and s2 theoretically as 0 mV for both, which is shown as V_{cal} in Table 3. We do not need to know the values of the permeability constants of ions for this calculation owing to the same argument given for the calculation of $V_{cal}(n1)$ and $V_{cal}(n2)$.

Table 3
The potential across Selemion

Notation	Left solution	Right solution	V_{exp} [mV]	V_{cal} [mV]
s1	0.10 M KCl	0.10 M KCl	0	0
s2	0.10 M NaCl	0.10 M NaCl	0	0
s3	0.10 M KCl	0.05 M KCl	−15	−18
s4	0.10 M KBr	0.10 M KI	+15	–
s5	0.10 M NaBr	0.10 M NaI	+12	–
s6	0.10 M KI	0.10 M NaI	0	0
s7	0.10 M KBr	0.10 M NaBr	0	0
s8	0.10 M KCl	0.05 M $CaCl_2$	−2	0
s9	0.05 M $CaCl_2$	0.05 M $FeCl_2$	−2	0
s10	0.033 M $FeCl_3$	0.05 M $FeCl_2$	+2	0
s11	0.10 M KCl:0.10 KI = 1:1 in vol	0.10 M KCl	+10	–

Notes. Left solution ≡ the type of solution and its concentration in the left compartment. Right solution ≡ the type of solution and its concentration in the right compartment. V_{exp} ≡ the experimentally measured potential across Selemion. V_{cal} ≡ the theoretically calculated potential across Selemion based on the membrane theory assuming it is quite permeable to cations and quite impermeable to anions. The left solution of s11 is a mixture of 0.10 M KCl and 0.10 M KI at a 1:1 volume ratio.

The experimentally obtained potentials of s3, s6, and s7 can be obtained through the HKG equation, too, under a certain assumption. Selemion contains a fixed cationic group; namely, it is a positively charged membrane. Therefore the positively charged particles, cations, are speculated hardly to permeate through Selemion compared with the negatively charged particles, anions. This speculation is interpreted as $P_{K^+} \ll P_{Cl^-}$ in case the HKG equation is applied to s3. Hence, Eq. (1) is transformed into

$$V_{cal}(s3) = (RT/F)\ln\left[\left(P_{K^+}[K^+]_l + P_{I^-}[Cl^-]_r\right) \Big/ \left(P_{K^+}[K^+]_r + P_{Cl^-}[Cl^-]_l\right)\right] \approx (RT/F)\ln\left[[Cl^-]_r/[Cl^-]_l\right]. \quad (8)$$

Since the potential measurement was performed within a few minutes after the completion of setting up the experimental apparatus depicted in Fig. 1, and $[Cl^-]_r$ and $[Cl^-]_l$ did not seem to change greatly from their initial concentrations. Therefore $[Cl^-]_l \approx 0.10$ M and $[Cl^-]_r \approx 0.05$ M. This gives $V_{cal}(s3) = -18$ mV, which is quite close to $V_{exp}(s3) = -15$ mV.

Applying the same argument to s6 and s7 results in expressions similar to Eq. (8), which are only different in that Cl^- is replaced by I^- for $V_{cal}(s6)$ and Br^- for $V_{cal}(s7)$. V_{cal} of s6 and s7 is 0 mV for both, the same as V_{exp} of s6 and s7.

The same argument applied to s3, s6, and s7 is applied to s4, resulting in

$$V_{cal}(s4) = (RT/F)\ln\left[\left(P_{K^+}[K^+]_l + P_{Br^-}[Br^-]_r + P_{I^-}[I^-]_r\right) \Big/ \left(P_{K^+}[K^+]_r + P_{Br^-}[Br^-]_l + P_{I^-}[I^-]_l\right)\right]. \quad (9)$$

We can immediately speculate on the relationship of $P_{K^+} \ll P_{Br^-}, P_{I^-}$ as to the permeability constants. Under this condition, Eq. (9) is reduced to

$$V_{cal}(s4) = (RT/F)\ln\left[\left(P_{Br^-}[Br^-]_r + P_{I^-}[I^-]_r\right) \Big/ \left(P_{Br^-}[Br^-]_l + P_{I^-}[I^-]_l\right)\right]. \quad (10)$$

Since we do not know the values of P_{Br^-} and P_{I^-}, we cannot proceed with further calculation. We cannot obtain the theoretical value of $V_{cal}(s4)$. But we can speculate that P_{Br^-} and P_{I^-} are different from each other, which might cause the nonzero potential of $V_{exp}(s4) = +15$ mV in Table 3. The same argument is applicable to explain the nonzero potential of s5, too.

The potentials of s8, s9, and s10 are quite close to 0 mV; we can virtually see them as 0 mV. The ionic species of the right compartment of s8 are different from those of the left compartment. However, considering the argument so far made, we can speculate that only the anions play a predominant role in the determination of potential behavior. The anion species and its concentration in both left and right compartment are exactly the same, Cl^- of 0.10 M. With these facts in mind, we can derive

$$V_{cal}(s8) \approx (RT/F)\ln\left[[Cl^-]_r/[Cl^-]_l\right]. \quad (11)$$

Since the potential measurement was performed within a few minutes after the completion of setting up the experimental apparatus depicted in Fig. 1, $[Cl^-]_r$ and $[Cl^-]_l$ did not seem to change greatly from their initial concentrations. Thus $V_{cal}(s8) \approx 0$ mV, which is in good agreement with $V_{exp}(n8) = -2$ mV. The same argument is applicable to s9 and s10, too.

The potential of s11 cannot be obtained theoretically through the HKG equation due to the same reason for the impossibility of the calculation of the potential of s4 and s5. But its nonzero potential is strongly speculated to be due to the difference of the values between P_{Cl^-} and P_{I^-}.

The dependence of the potential across the semipermeable membranes on the ionic species shown in Tables 1–3 has been quite well known [2], and we could well explain these potential behaviors employing the membrane theory. It impresses us that the membrane theory is completely validated. Next, we examine the validity of the adsorption theory based on the modified Colacicco experiment [1].

3.2. Implications of Colacicco's experiment

Before showing our experimental results, we would like to review the Colacicco experiment [1] by employing the interpretation of Ling [2,4,5,8]. The following description is quoted particularly from Ref. [5], authored by Ling.

Colacicco performed an investigation on the potential difference between two aqueous KCl solutions separated by an oil layer. He measured the potential between 1 and 100 mM KCl solutions separated by an oil layer. The membrane theory predicts a potential of 119 mV. Yet in fact, he observed 0 mV. This is in conflict with the membrane theory. One may argue that this disagreement is due to the impermeability of

the oil layer to both K^+ and Cl^-. Then Colacicco introduced into one compartment a small amount of anionic detergent, sodium dodecylsulfate, or SDS. SDS is an electrolyte and can create free cations in aqueous solution through its dissociation. The hydrocarbon tail of SDS is anchored in the oil layer due to its hydrophobicity, while its polar head is exposed to the aqueous solution phase due to its hydrophilicity. Therefore an anionic molecular layer of SDS is formed at the interface of aqueous solution and oil layers. With the introduction of SDS, Colacicco observed a nonzero, to be precise, a positive potential with respect to the other compartment. He also observed that this potential was sensitive to the concentration of K^+ in the compartment containing SDS but insensitive to that in the other compartment; furthermore it was insensitive to the concentration of Cl^- in both compartment. This finding suggests that this potential was created only at the interface of aqueous solution and oil layers with SDS, and it is more as if the potential is determined independent of the compartment without SDS.

He performed another experiment. He introduced into the compartment a small amount of cationic detergent, cetyltrimethylammonium bromide or CTAB, instead of SDS. CTAB is an electrolyte and can create a free anion in aqueous solution through its dissociation. The tail of CTAB is anchored in the oil layer due to its hydrophobicity, while its polar head is exposed to the aqueous solution phase due to its hydrophilicity. Therefore a cationic molecular layer of CTAB is formed at the interface of the aqueous solution and oil layers. With the introduction of CTAB, Colacicco observed a nonzero, to be precise, a negative potential with respect to the other compartment. He also observed that this potential was sensitive to the concentration of Cl^- in the compartment containing CTAB but insensitive to that in the other compartment; furthermore it was insensitive to the concentration of K^+ in both compartments. This finding suggests that this potential was created only at the interface of the aqueous solution and oil layers with CTAB, and the solution in the other compartment does not appear to be involved in the potential generation. So the potential is determined independent of the compartment without CTAB, as in the case of SDS introduction.

Why did the introduction of SDS (CTAB) cause the nonzero potential? Does SDS (CTAB) turn the oil layer into a membrane permeable to K^+ (Cl^-)? Such a speculation is incompatible with the experimentally observed insensitivity of the potential to the concentration of K^+ (Cl^-) in the compartment containing no SDS (no CTAB). However, without the selective permeability of the membrane to ions, the nonzero membrane potential cannot be generated according to the membrane theory.

Colacicco carried out a further experiment and found remarkable evidence defying the membrane theory. He combined the two experiments described above. He introduced SDS into one compartment and CTAB into the other compartment. If the potential generation by the introduction of either SDS or CTAB is due to the alteration of oil layer to acquire permeability to K^+ or Cl^-, respectively, the oil having both SDS and CTAB layers on its surfaces is fully permeable to both K^+ and Cl^-. So according to the membrane theory, the expected potential is 0 mV in this case regardless of the concentration of KCl in both compartments. However, Colacicco observed a quite large nonzero potential, which was close to the sum of the potentials observed in case only SDS was introduced and in case only CTAB was introduced. So Colacicco's experiment suggests that the potential long called the membrane potential is not a membrane origin potential. The potential is not determined by the selective permeability of the membrane. It is solely determined by the individual interface between the oil layer and the KCl solution. Ling suggests that the potential generation originates from the adsorption of ions onto the SDS layer and CTAB; namely, the membrane potential is, in fact, of adsorption origin, that is, an adsorption potential [2,4,5,8]. The presence of adsorption sites and ions to be adsorbed onto such adsorption sites generates the potential. Not only Ling but some other people also more or less have advocated or sided with the adsorption theory [1,3,7,10–12]. However, their efforts have been dismissed up until now. So we reconsider our observation with the adsorption theory in mind again in the subsequent sections.

3.3. Reconsideration of membrane potential

In order to enhance the implication of Colacicco's work [1] and validate the adsorption theory further, we performed the following experiments extending his work.

3.3.1. Absolute potential values

We measured the absolute potential values of several different types of ionic solutions in contact with Nafion (or Selemion). The apparatus used is the same as depicted in Fig. 1, but the left compartment is filled with the agar gel containing the saturated KCl. Through the intermediary of Nafion (or Selemion), this agar gel adjoins to the ionic solution in the right compartment. Therefore the potentials were all measured with respect to the solid agar gel phase. Table 4 shows the potentials we measured. The absolute potentials in Table 4 behave differently according to their ionic species and concentrations, and they do not seem to obey the predictions of the membrane theory. For the sake of simplicity, here we assume that there exists an invisible thin saturated 3.3 M KCl solution layer between the agar phase and Nafion (Selemion) as depicted in Fig. 2. Then we tried applying the membrane theory [2,4,6,8] to theoretically calculate the potentials in Table 4. The calculated results disagree with V_{exp}. For example, the calculated potential of n41 is +150 mV; this is totally different from $V_{exp}(n41) = +99$ mV. The calculated potential of others, V_{cal}, are also listed in Table 4 for the purpose of reference.

Table 5 shows some potential data given in Tables 2 and 3; these data are redesignated in Table 5, along with the additionally measured potentials of n512 and n513 em-

Table 4
The potential across Nafion and Selemion with respect to the agar gel containing saturated KCl

Notation	Left solution	Right solution	V_{exp} [mV]	V_{cal} [mV]
n41	saturated KCl	0.01 M KCl	+99	+150
n42	saturated KCl	0.05 M KCl	+86	+108
n43	saturated KCl	0.10 M KCl	+74	+90
n44	saturated KCl	0.01 M KI	+113	+150
n45	saturated KCl	0.05 M KI	+91	+108
n46	saturated KCl	0.10 M KI	+78	+90
n47	saturated KCl	0.01 M KBr	+104	+150
n48	saturated KCl	0.05 M KBr	+87	+108
n49	saturated KCl	0.10 M KBr	+76	+90
n410	saturated KCl	0.01 M NaI	+103	–
n411	saturated KCl	0.05 M NaI	+94	–
n412	saturated KCl	0.10 M NaI	+86	–
n413	saturated KCl	0.01 M $CaCl_2$	+108	–
n414	saturated KCl	0.05 M $CaCl_2$	+105	–
n415	saturated KCl	0.10 M $CaCl_2$	+84	–
s41	saturated KCl	0.01 M KCl	−107	−150
s42	saturated KCl	0.05 M KCl	−92	−108
s43	saturated KCl	0.10 M KCl	−77	−90
s44	saturated KCl	0.01 M KI	−119	–
s45	saturated KCl	0.05 M KI	−88	–
s46	saturated KCl	0.10 M KI	−50	–
s47	saturated KCl	0.01 M KBr	−115	–
s48	saturated KCl	0.05 M KBr	−82	–
s49	saturated KCl	0.10 M KBr	−66	–
s410	saturated KCl	0.01 M NaI	−121	–
s411	saturated KCl	0.05 M NaI	−86	–
s412	saturated KCl	0.10 M NaI	−53	–
s413	saturated KCl	0.01 M $CaCl_2$	−115	−132
s414	saturated KCl	0.05 M $CaCl_2$	−104	−90
s415	saturated KCl	0.10 M $CaCl_2$	−74	−72

Notes. Left solution ≡ the saturated KCl contained in agar gel. Right solution ≡ the type of solution and its concentration in the right compartment. V_{exp} ≡ the experimentally measured potential across the membranes. V_{cal} ≡ the theoretically calculated potential across the membranes based on the membrane theory. Nafion was used as a membrane separating the agar gel and an ionic solution for the potential measurement of n41–n415. Selemion was used as a membrane separating the agar gel and an ionic solution for the potential measurement of s41–s415.

ploying exactly the same method for the measurement of the potentials shown in Table 2. We calculated the potentials in Table 5 using the potential data in Table 4. For example, V_{cal}(n53) in Table 5 was calculated as $V_{cal}(n53) = V_{exp}(n42) - V_{exp}(n43) = +12$ mV. In the same manner, the other V_{cal} was obtained and given in Table 5. In spite of the large disagreement between the experimental results in Table 4 and their theoretical predictions by the membrane theory, V_{cal} in Table 5 calculated using V_{exp} in Table 4 is in good agreement with the corresponding V_{exp} in Table 5. So we try to explain the behavior of experimentally measured potential, V_{exp}, shown in Tables 4 and 5.

Ling suggests that the ion adsorption onto the spatially fixed adsorption sites dominates the potential behavior in the ionic solution systems [2,4,8]. Taking up V_{exp}(n51), we apply Ling's concept to it. Ionic solutions in the left and right compartments directly contact the negatively charged membrane Nafion. So Nafion offers a large number of negatively

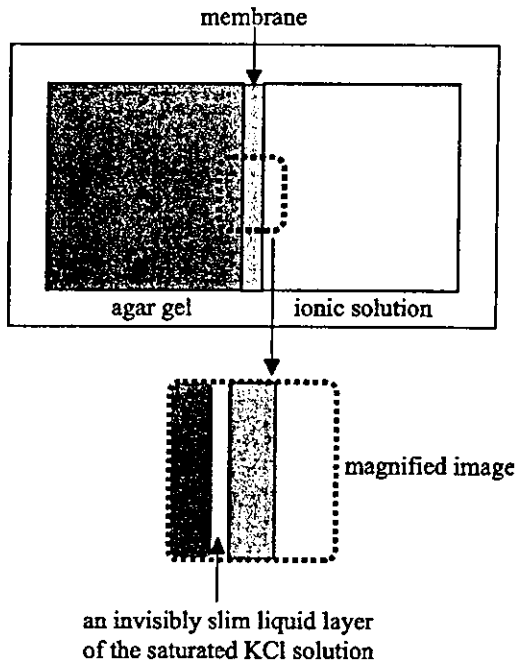

Fig. 2. The magnified image of an invisibly thin phase of saturated KCl solution speculated to be probable to occur.

Table 5
The potential across Nafion and Selemion

Notation	Left solution	Right solution	V_{exp} [mV]	V_{cal} [mV]
n51	0.01 M KCl	0.01 M KCl	0	0
n53	0.10 M KCl	0.05 M KCl	+17	+12
n54	0.10 M KBr	0.10 M KI	+1	+2
n56	0.10 M KI	0.10 M NaI	+9	+8
n510	0.10 M KCl	0.05 M $CaCl_2$	+10	+10
n512	0.10 M KCl	0.10 M KI	+2	+4
n513	0.10 M KCl	0.10 M NaI	+10	+12
s51	0.01 M KCl	0.01 M KCl	0	0
s53	0.10 M KCl	0.05 M KCl	−15	−15
s54	0.10 M KBr	0.10 M KI	+15	+16
s56	0.10 M KI	0.10 M NaI	0	−3
s58	0.10 M KCl	0.05 M $CaCl_2$	−2	+3

Notes. Left solution ≡ the type of solution and its concentration in the left compartment. Right solution ≡ the type of solution and its concentration in the right compartment. V_{exp} ≡ the experimentally measured potential across the membranes. V_{cal} ≡ theoretically calculated potential using V_{exp} in Table 4. Nafion was used as a membrane separating the agar gel and an ionic solution for the potential measurement of n51–n513. Selemion was used as a membrane separating the agar gel and an ionic solution for the potential measurement of s51–s58.

charged adsorption sites to the free cations, where they cannot be adsorption sites to the anions due to electrostatic repulsion. Therefore the potential is generated at the interfaces between the surfaces of Nafion exposed to ionic solutions in the left and right compartments. The degree of adsorption of cations onto the Nafion surfaces should depend on the concentration of cations from the view of the chemical reaction. Thus the generated potential across Nafion, V_{exp}(n51), is determined by two independent potentials, where one is

Table 6
The potential across the membrane consisting of a dialysis membrane, an agar gel containing saturated KCl, and a Nafion or Selemion

Notation	Left solution	Right solution	V_{exp} [mV]	V^l_{exp} [mV]	V^r_{exp} [mV]
n61	0.01 M KCl	0.10 M KCl	+84	0	+84
n62	0.05 M KCl	0.10 M KCl	+84	+1	+84
n63	0.10 M KCl	0.10 M KCl	+84	+1	+83
n64	0.10 M KCl	0.01 M KCl	+126	+1	+125
n65	0.10 M KCl	0.05 M KCl	+97	+1	+96
n66	0.10 M KCl	0.10 M KCl	+84	0	+84
s61	0.01 M KCl	0.10 M KCl	−76	0	−76
s62	0.05 M KCl	0.10 M KCl	−76	0	−76
s63	0.10 M KCl	0.10 M KCl	−75	0	−75
s64	0.10 M KCl	0.01 M KCl	−105	0	−105
s65	0.10 M KCl	0.05 M KCl	−87	0	−86
s66	0.10 M KCl	0.10 M KCl	−76	0	−76

Notes. Left solution ≡ the type of solution and its concentration in the left compartment. Right solution ≡ the type of solution and its concentration in the right compartment. V_{exp} ≡ the experimentally measured potential across the membrane consisting of a dialysis membrane, an agar gel containing saturated KCl, and a Nafion. V^l_{exp} ≡ the experimentally measured potential between the left compartment and the agar gel phase V^r_{exp} ≡ the experimentally measured potential between the right compartment and the agar gel phase. Nafion was used as a membrane separating the solid agar containing saturated KCl and an ionic solution for the potential measurement of n61–n66. Selemion was used as a membrane separating the solid agar containing saturated KCl and an ionic solution for the potential measurement of s61–s66. n66 is the same as n63. s66 is the same as s63.

determined at the interface between the left solution and the left surface of Nafion and the other one is determined at the interface between the right surface of Nafion and the right solution. This explanation is applicable to the other V_{exp} in Tables 4 and 5, too.

3.3.2. *Influence of the ion concentration and the membrane components on the potential generation*

We measured the potential generated between two adjoining KCl solutions through the intermediary of a membrane consisting of a dialysis membrane, an agar gel containing the saturated KCl, and a Nafion as depicted in Fig. 3. What is important here is that the solution in the left compartment is exposed to a quite permeable neutral dialysis membrane, while the solution in the right compartment directly contacts negatively charged membrane; that is, the solution in the left compartment can be regarded as virtually in direct contact with the agar gel. From the discussion in Section 3.3.1, the dialysis membrane has little influence on the potential. Therefore it merely plays a preventive role in the disintegration of the agar gel. The observed potentials, V_{exp}, are summarized in Table 6.

As to n61–n66 in Table 6, employing Nafion as a semipermeable polymer membrane, we can know that V_{exp} is indifferent to the KCl concentration in the left compartment from the potential behavior of n61, n62, and n63. On the other hand, we can know that it is quite sensitive to the KCl concentration in the right compartment from the potential behavior of n64, n65, and n66. Therefore the right compartment dominates the potential behavior. What is different between the right and the left compartments is the type of membrane used, that is, either dialysis membrane or Nafion. Their potentials depend solely on the right compartment where there is an interface between KCl solution and Nafion. Therefore the relationship between the ionic solution

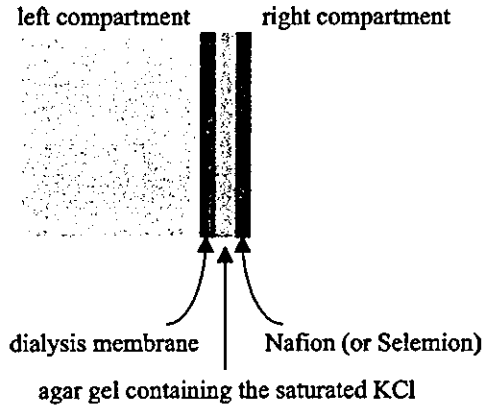

Fig. 3. The structure of membrane employed.

and the charged membrane is speculated to be responsible for the potential. This is what the adsorption theory predicts [2–5,7,8,10–12]. The same argument is applicable to the potential behavior of s61–s66 in Table 6. Their potential behavior depends solely on the right compartment, where there is an interface between the KCl solution and the positively charged membrane, Selemion. We also measured the potentials between the left compartment and the agar gel phase, V^l_{exp}, and between the agar gel phase and the right compartment, V^r_{exp}, as depicted in Fig. 4. The results are also shown in Table 6. Virtually we can interpret them as $V^l_{exp} = 0$ mV and $V_{exp} = V^r_{exp}$. Namely, the potential, V_{exp}, is undoubtedly solely determined at the interface between the right solution and Nafion (or Selemion). And we would like to add some words on this potential behavior. The individual potential of V_{exp} in Table 6 is maintained almost perfectly constant during the potential measurement. The potential deviation was within ±1 mV. This means that the KCl concentration variation in the left compartment concerning n61–n63 truly does not have even a slight influence on the behavior of V_{exp}. It is

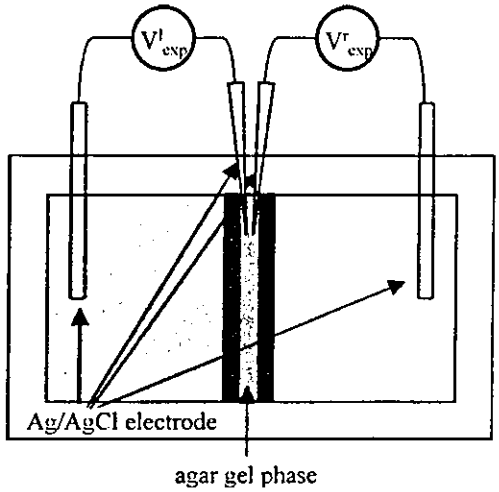

Fig. 4. The definition of V^r_{exp} and V^l_{exp}. V^r_{exp} is the potential of the right compartment with respect to the agar gel phase, and V^l_{exp} is the potential of the agar gel phase with respect to the left compartment.

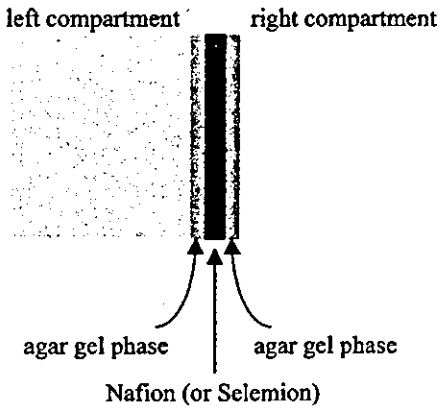

Fig. 5. The membrane of Nafion (or Selemion) sandwiched between the agar gels containing the saturated KCl solutions.

also true for s61–s63 that KCl concentration variation in the left compartment does not have any influence on the behavior of V_{exp} at all. What is important is not the selective permeability of the membrane but the existence of adsorption sites of Nafion and Selemion exposed to the ionic solution.

In order to further support the arguments above, we performed the following additional experiment. Two KCl solutions were separated by Nafion (or Selemion) fully embedded in the agar gel containing the saturated KCl as depicted in Fig. 5. We measured the potential of these KCl solutions across these membranes. The results are shown in Table 7. Two KCl solutions both in the left and the right compartments do not directly contact Nafion (or Selemion). According to the adsorption theory [1–5,7,8,10–12], the disparity of KCl concentration between two compartments cannot generate a nonzero potential because of no direct exposure of adsorption sites of Nafion (or Selemion) to KCl solution. Actually, we observed 0 mV or almost 0 mV potentials as in Table 7. It agrees with the adsorption theory, while it disagrees with the membrane theory.

Table 7
The potential across Nafion (or Selemion) embedded in the agar gel containing the saturated KCl

Notation	Left solution	Right solution	V_{exp} [mV]
n71	0.01 M KCl	0.10 M KCl	0
n72	0.05 M KCl	0.10 M KCl	0
n73	0.10 M KCl	0.10 M KCl	0
s71	0.01 M KCl	0.10 M KCl	+1
s72	0.05 M KCl	0.10 M KCl	+1
s73	0.10 M KCl	0.10 M KCl	+1

Notes. Left solution ≡ the type of solution and its concentration in the left compartment. Right solution ≡ the type of solution and its concentration in the right compartment. V_{exp} ≡ the experimentally measured potential. Employed membrane is Nafion embedded in the agar gel containing the saturated KCl for n71–n73. Employed membrane is Selemion embedded in the agar gel containing the saturated KCl for s71–s73.

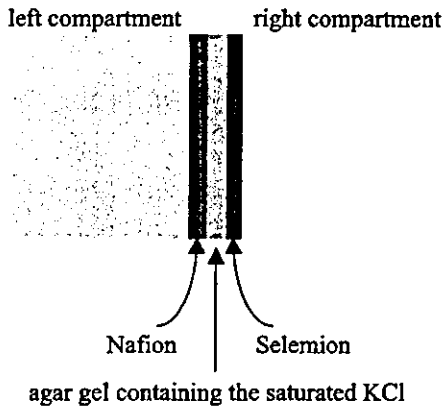

Fig. 6. The structure of the membrane employed.

3.3.3. *Combination of Nafion and Selemion on the potential generation*

If the adsorption theory is right rather than the membrane theory, we must be able to observe a large potential by employing the membrane with the positively charged sites on one side and the negatively charged sites on the other side as Colacicco observed [1,2,4,5,8]. We performed the following experiments to see if we can actually observe this. We measured the potential across two KCl solutions separated by the membrane consisting of a Nafion, an agar gel containing saturated KCl, and a Selemion as depicted in Fig. 6. In this case, the membrane theory predicts 0 mV as the observed potential. However, the actually observed potentials, V_{exp}, shown in Table 8, are totally different from the prediction by the membrane theory. One plausible explanation for this potential behavior could be derived from the Colacicco experiment explained in Section 3.2 [1,2,4, 5,8]. Colacicco observed the large nonzero potential generated between two KCl solutions across the oil layer with SDS and CTAB. The potential he observed was merely the sum of two potentials generated at the interfaces between KCl solution and SDS layer and between KCl solution and CTAB layer. This explanation could explain the potential behavior of V_{exp} in Table 8 in line with adsorption theory.

Table 8
The potential across the membrane consisting of Nafion, agar gel containing saturated KCl, and Selemion

Notations	Left solution	Right solution	V_{exp} [mV]	V_{cal} [mV]	V^l_{exp} [mV]	V^r_{exp} [mV]
ns1	0.10 M KCl	0.10 M KCl	−160	−151	−81	−78
ns2	0.01 M KCl	0.10 M KCl	−179	−176	−98	−78
ns3	0.10 M KCl	0.01 M KCl	−198	−181	−81	−114
ns4	0.01 M KCl	0.01 M KCl	−217	−206	−99	−116

Notes. Left solution ≡ the type of solution and its concentration in the left compartment where the left solution directly contacts Nafion. Right solution ≡ the type of solution and its concentration in the right compartment where the right solution directly contacts Selemion. V_{exp} ≡ the experimentally measured potential across the membrane consisting of Nafion, agar gel containing saturated KCl, and Selemion. V_{cal} ≡ theoretically calculated potential following Colacicco's procedure. V^l_{exp} ≡ the potential between the left compartment and the agar phase. V^r_{exp} ≡ the potential between the right compartment and the agar phase.

Following the Colacicco scheme [2], we theoretically calculated the potential, V_{cal}, for ns1–ns4. Using the potential data shown in Table 4, for instance, V_{cal}(ns1) is calculated as $V_{cal}(ns1) = V_{exp}(s43) - V_{exp}(n43) = -151$ mV. All other potentials were calculated in the same manner and are summarized in Table 8. For all the cases, V_{cal} is quite close to V_{exp}. Furthermore, we measured V^l_{exp} and V^r_{exp} following the same procedure as described in Section 3.3.2. The results are given in Table 8, too. Obviously, V_{exp} is given by the sum of V^l_{exp} and V^r_{exp}. V^l_{exp} depends on KCl concentration in the left compartment and is independent of the condition of the right compartment. V^r_{exp} depends on KCl concentration in the right compartment and is independent of the condition of the left compartment. So all the potential behaviors we have observed, V_{exp}, V^l_{exp}, and V^r_{exp}, are indeed determined at the interfaces between the agar gel and Nafion and between the agar gel and Selemion, not by the selective permeability of the membrane.

3.4. Reinterpretation of the membrane potential

Extending Colacicco's work [1], we performed several experiments. Considering the results obtained up until here along with the results Colacicco obtained in his own research, the passage of ions through the membrane does not appear to affect the potential generation. Our observation suggests that one compartment containing the solution has its own potential independent of the other compartment's condition. What we measured as the membrane potential is merely the combined potentials of the two compartments, as Colacicco observed long ago. For the generation of nonzero potential, what is important must be the surface adsorption of ions on the membrane, as suggested by the proponents of the adsorption theory. In order to strongly support the meaning of ion adsorption onto the membrane the following experiment was performed.

Cheng experimentally showed that the change of ratio of the number of adsorption sites on one membrane surface to that on the opposite membrane surface, which separate two ionic solutions, can cause a potential change [11]. This strongly suggests that the adsorption sites on the membrane surfaces are involved in the nonzero potential generation, rather than the selective permeability of the membrane; that is, his research results support the adsorption theory. With

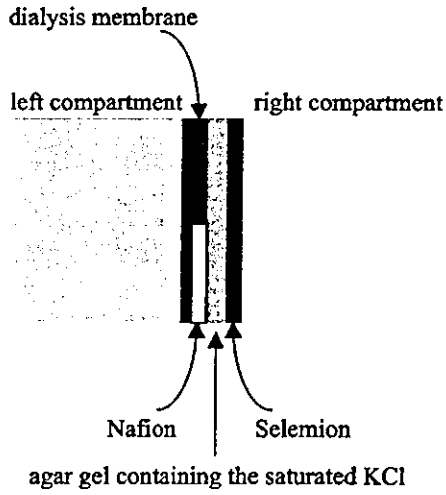

Fig. 7. The structure of the membrane employed. It has three layers. The left side consists of dialysis membrane, half of which is covered with Nafion. The middle portion is an agar gel containing the saturated KCl. The right side consists of Selemion.

Cheng's work in mind, we performed the following experiment. A membrane consisting of dialysis membrane, Nafion, Selemion, and agar gel containing saturated KCl was prepared; its structure is depicted in Fig. 7. It separates two KCl solutions. The left side of the membrane consists of a dialysis membrane half of which is covered with Nafion (see Fig. 7). This left side surface of the membrane can be regarded as quite permeable because half of it is covered with dialysis membrane only, and this area directly contacts the agar gel and KCl solution.

Table 9 is the results we obtained. dns1 and dns2 are different from each other only in the KCl concentration in the left compartment. Since the left surface of the membrane is quite permeable to ions, the semipermeable membrane is virtually Selemion only. Therefore according to the membrane theory, we can expect a potential decrease with the increase of KCl concentration in the left compartment. However, the experimentally obtained potentials of V_{exp}(dns1) and V_{exp}(dns2) have the opposite relationship. This must be caused by the role of Nafion as an adsorption site for K^+; this concept agree with the adsorption theory.

The potential of dns1 and dns2 seem to decrease slowly with time. Therefore lower potentials than V_{exp}(dns1) and